Chinese Chemical Letters 35 (2024) 109532

Contents lists available at ScienceDirect

Chinese Chemical Letters

journal homepage: www.elsevier.com/locate/cclet

N,O-Bidentated difluoroboron complexes based on pyridine-ester enolates: Facile synthesis, post-complexation modification, optical properties, and applications

Chaochao Jin[a], Kai Li[b,*], Jiongpei Zhang[a], Zhihua Wang[a,*], Jiajing Tan[a,*]

[a] College of Chemistry, Beijing University of Chemical Technology (BUCT), Beijing 100029, China
[b] College of Materials Science and Engineering, Shenzhen University, Shenzhen 518055, China

ARTICLE INFO

Article history:
Received 9 November 2023
Revised 4 January 2024
Accepted 12 January 2024
Available online 24 January 2024

Keywords:
N,O-Bidentate BF_2 complexes
Aggregation-induced emission
Large Stokes shift
Post-complexation modification
Reversible acidic vapor sensor

ABSTRACT

An array of pyridine-ester enolate based organoboron complexes has been designed and synthesized *via* a one-pot cascade of Pd-catalyzed α-arylation and BF_2 complexation. The rapid structure-activity relationship (SAR) studies indicated that unsymmetrical *N,O*-chelated BF_2 complexes were highly fluorescent in solid state, and exhibited large Stokes shifts, excellent photostability, along with insensitivity to pH. The α-aryl group could not only modulate the electronic effect but also inhibit the intermolecular π-π stacking to promote the aggregation-induced emission (AIE) effect. DFT calculations and experiments identified that the intramolecular charge transfer properties of these *N,O*-chelates could be switched by the modification of substituents, resulting tunable fluorescence wavelengths. Furthermore, post-complexation modification was accomplished, including Suzuki-Miyaura cross-coupling, Buchwald-Hartwig amination, oxidative cleavage, along with a unique triple substitution reaction involving propargyl Grignard reagents. The exemplificative application of dimethylamine substituted boron complex as a reversible acidic vapor sensor was also demonstrated.

The emerging demand for luminescent materials, capable of functioning in diverse optoelectronic devices such as organic light-emitting diodes (OLEDs) or light-emitting electrochemical cells (OLECs), as well as for utility in optical sensing applications in biological and supramolecular systems, continue to drive significant efforts toward discovering novel fluorescent compounds and developing their practical synthetic methods [1–4]. In particular, organoboron complexes have been extensively investigated as fluorescent dyes in recent years [5]. Among them, boron dipyrromethene (BODIPY) stand out for their favorable characteristics, including high quantum yield, narrow emission bands, and excellent photo-stability. These features make them ideal candidates for a myriad of applications, ranging from fluorescence imaging reagents, sensitizers for solar cells, and photodynamic therapy [6–10]. However, the inherent symmetric and planar configuration of BODIPY type compounds often led to small Stokes shifts and aggregation-caused quenching (ACQ), limiting their utility in certain scenarios whereas necessitating the structural engineering to enhance their functions [11,12].

The development of efficient solid-state luminescent materials is also crucial for advancements in optoelectronic materials, devices as well as chemical and biological sensors [13–17]. First identified by Tang and colleagues in 2001, the phenomenon of Aggregation-Induced Emission (AIE) has been extensively observed in molecules possessing highly twisted conformations [18]. These AIE-active luminophores, or 'AIEgens', display subdued luminescence in solution but enhanced emission upon aggregation or transition to the solid-state, primarily due to restricted intramolecular motion (RIM) [19,20]. Accordingly, the applications of AIEgens have been witnessed across various sectors, including bioimaging [21,22], sensing [23], OLEDs [24], and other optically-active technologies [25]. In contrast, BODIPY-derived fluorescent complexes often suffered from ACQ owing to their planar geometries and propensity for intermolecular π-π stacking interactions, significantly curtailing their utilities. Despite substantial advancements in recent years [26–31], the rational design and optimization of structural variations of BODIPYs for better performance remain a challenging yet pivotal endeavor.

Compared to *N,N*-bidentate BODIPY counterpart, *N,O*-bidentate complexes that share structural similarities often possess distinct

* Corresponding authors.
E-mail addresses: kaili@szu.edu.cn (K. Li), zhwang@mail.buct.edu.cn (Z. Wang), tanjj@mail.buct.edu.cn (J. Tan).

https://doi.org/10.1016/j.cclet.2024.109532
1001-8417/

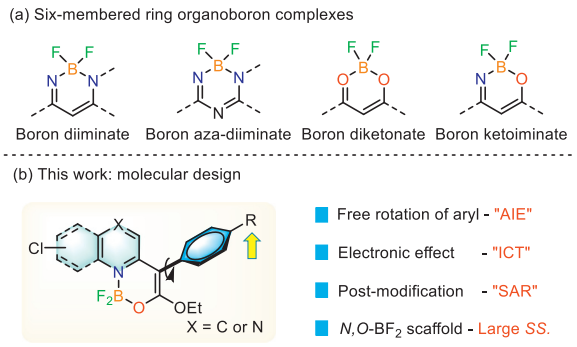

Scheme 1. Working hypothesis.

properties but remained relatively unexplored (Scheme 1a) [32–40]. For instance, research groups led by Wang, Ziessel, and others have respectively demonstrated that phenol-based *N,O*-chelated boron complexes could display significant fluorescence and thus show promise in applications such as organic light-emitting diodes or fluorescent labeling reagents [41–46]. Chujo *et al.* reported a series of organoboron dyes with ketoiminate and diiminate as ligands, which exhibited mechanochromic properties [47–50]. Motivated to fill the apparent gap, we recognized that our long-term research on fluorescent materials, as well as recent serendipity finding on *N,O*-chelated palladium complex might be transferred to boron complexation, eliciting the design and development of new type of fluorescent compounds [51–54]. Specifically, we envisioned the enolizable character of ester group might empower it as a bidentate *N,O*-ligand to chelate the boron atom, leading to unsymmetrical *N,O*-BF_2 scaffold that might offer improved Stokes shift and mitigate self-absorption issues (Scheme 1b). Besides, the pyridine ring could act as a strong electron acceptor upon coordination with BF_2, facilitating the design and construct the D-π-A units [55]. Furthermore, introducing aryl groups to α-position of esters could not only alter the push-pull effect within the complex, but also inhibit intermolecular π-π stacking by inducing twisted propeller-shaped conformations [56]. Nevertheless, we herein would like to report the proof-of-concept execution of the aforementioned ideas, and present a series of readily accessible unsymmetrical BF_2 fluorophores that incorporate *N*-heteroarene derivatives. The streamlined one-pot-two-step synthesis and post-complexation modification enabled the variation of *N*-heterocyclic framework and α-aryl groups in high efficiency. In addition to offering the carbonyl moiety for coordination, the ester group within the substrate scaffold could serve as an additional reactive site for further modifications. Overall, these new complexes demonstrated excellent photo/pH stability, unique photophysical properties, and showed promise in applications as reversible acidic vapor sensors.

We first telescoped the synthesis cascade comprising Pd-catalyzed α-arylation of α-(2-pyridinyl)acetates and fluorine-boron complexation with $BF_3{\cdot}Et_2O$ in the presence of hexamethyldisilazane (HMDS). After extensive investigations, we established a one-pot, two-step protocol, providing the BF_2 complex **3a** in 86% yields, which displayed strong fluorescence and thus prompted us to further explore their SAR (Scheme 2). Indeed, our method was amenable to both pyridine, quinoline and quinoxaline scaffolds, tolerating both electron-donating groups (EDGs) and electron-withdrawing groups (EWGs). The obtained complexes were stable to and successfully isolated using silica column chromatography, affording solid products with satisfactory yields. Comprehensive structural analyses were performed using ^{1}H NMR, ^{13}C NMR, ^{19}F NMR, HRMS, and X-ray crystal analysis.

These dyes exhibit excellent optical properties with a strong broad absorption and intense emission in visible regions in dichloromethane (DCM) (Table 1). Compounds **3a-3j** displayed two obvious absorption bands in solvents: the one in 310–330 nm range is assigned as π-π^* transition, while the other one in the low-energy region corresponds to the intramolecular charge transfer (ICT) transition [57,58]. Compared to the *meso*–phenyl substituted BODIPY [59], **3a-3j** showed similar level of quantum yields in solution, but much larger Stokes shifts (84–121 nm), which was critical for avoiding the detrimental effects of self-absorption. The installation of dimethylamine, diphenylamine, or carbazole group to the *para* position of aryl ring led to a gradual red shift in the absorption and emission bands (Fig. 1 and Fig. S1 in Supporting information), whereas the electron-withdrawing trifluoromethyl group shifted the emission to blue. In addition, the quinoline or quinoxaline based fluorescent molecules (**3f-3j**) display longer emission wavelengths than the pyridine-based counterparts (**3a-3e**). Compared with data in solution, the molecular aggregation effects in solid states restrict the free rotation of the α-aryl groups, empowering more red-shifted emission and significantly improved quantum yields. Moreover, the emission of our fluorophores can be tuned on purpose by modulating the substitution group or ligand scaffold.

The optical properties of **3a** were measured in different solvents. As the solvent polarity increased from toluene to glycol, a tiny shift in the maximum absorption band was observed, indicating a stable ground state [60]. The fluorescence emission maximum of **3a** varied with changes in solvent polarity. As the solvent polarity increased from hexane to acetonitrile, a gradual decrease in the emission intensity of **3a** was observed (Figs. 2a and b). This

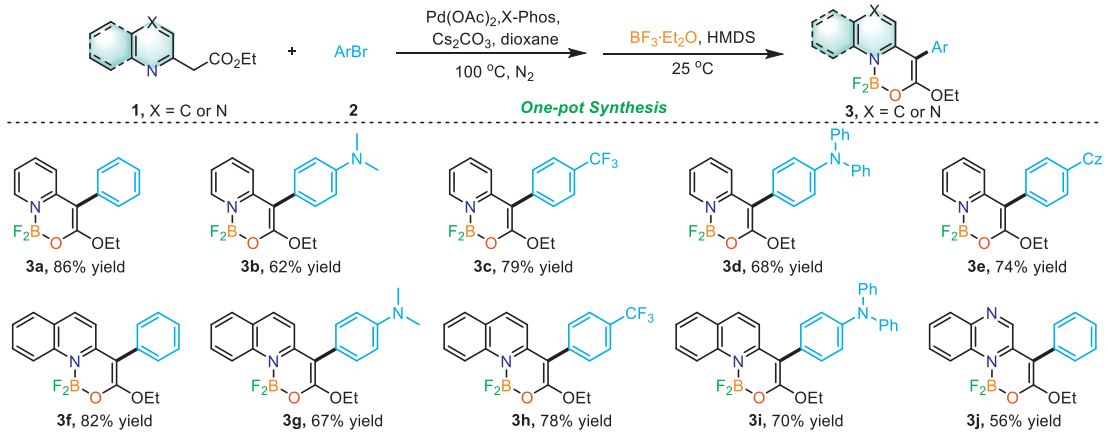

Scheme 2. One-pot syntheses of complexes **3** from **1** to **2**. Cz = Carbazole.

Table 1
Photophysical properties of compounds **3a-3i** in dichloromethane and solid powder.

Compound	Dichloromethane[a]					Powder		
	λ_{abs} (nm)/ε [b]	λ_{em} (nm)	Stokes shift (nm) [c]	Φ_f (%)[d]	τ (ns)	λ_{em} (nm)	Φ_f (%)[d]	τ (ns)
3a	375 (59400)	483	108	3.6	1.5	478	33	3.8
3b	384 (32500)	490	106	0.6	<1	494	32	4.9
3c	372 (30600)	461	89	12	2.6	456	23	3.2
3d	380 (39600)	496	116	1	<1	521	8	7
3e	381 (20800)	496	88	21	3.4	503	36	5.4
3f	408 (63100)	492	84	0.5	<1	494	13	2.2
3g	412 (33400)	517	105	0.3	4.9	507	35	1.7
3h	404 (46800)	487	83	1.5	<1	482	14	<1
3i	409 (22300)	530	121	1.1	3.6	541	13	1.9
3j	441 (33200)	540	99	2.3	1.8	563	28	2.6

[a] Molar absorption coefficients of the absorption maxima at longer wavelength region.
[b] The spectra were recorded in DCM ($c = 1.0 \times 10^{-5}$ mol/L) at room temperature.
[c] Energy gap between the absorption and emission maxima in DCM solution.
[d] Absolute quantum yield determined by calibrated integrating sphere system.

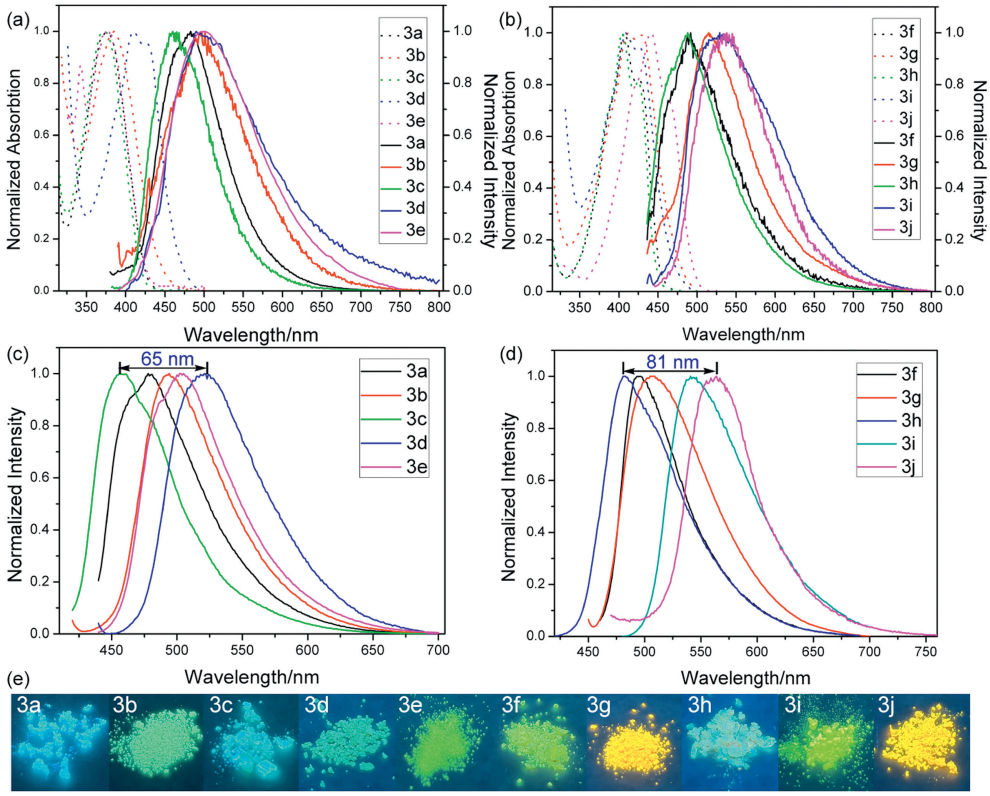

Fig. 1. (a, b) Absorption (dotted line) and emission (solid line) spectra of **3a-3e** and **3f-3i** in dichloromethane. (c, d) Emission spectra of **3a-3e** and **3f-3i** in solid powder state; (e) Insert picture: **3a-3j** under the 365 nm UV light.

decrease could be attributed to the ICT process from the phenyl ring to the boron coordinated pyridine moiety. In high-viscosity solvents such as glycol, **3a** exhibited significantly enhanced luminescence intensity (Fig. 2b). In a THF-H_2O solvent system, the emission intensity of **3a** also increased with increasing water fraction (f_w). When the f_w exceeded 70%, visible aggregates were formed with a particle diameter of 412 nm (Figs. 2c and d). This observed AIE effect arises from the conformational locking of phenyl rotors in the assembled state, leading to suppressed non-radiative relaxation.

Next, X-ray crystallographic analysis was performed to better understand the relationship between structure and solid-state emission properties (Fig. 3, Tables S1 and S2 in Supporting information). Single crystal analysis reveals that the molecules are stacked in opposite directions, allowing for greater slippage that reduces stacking (slip angel ranges from 37.10° to 60.11°, Figs. S7-S12 in Supporting information). As depicted in Fig. 3a, the C_5-C_6 and C_6-C_7 bond distances are 1.435 and 1.372 Å, respectively. These values suggest that the ester enolization enable the formation of C=C bond between C_6 and C_7 [61]. The central boron atom has a slightly distorted tetrahedral geometry with B-F, B-N and B-O distances of 1.370, 1.568 and 1.456 Å, respectively (Table S3 in Supporting information). In these dyes, the substituted benzene rings maintain an almost vertical orientation relative to the NBO core, with dihedral angles ranging from 56° to 78°, as indicated in Table S3. Notably, no face-to-face π-π stacking was observed but multiple short interatomic contacts (C_9-H_9···F_1 (2.695 Å), (C_9-H_9···O_1 (2.621 Å) instead in **3a**. These weak interactions can restrict the molecular conformations by locking the molecules into aggregated structures as well as attenuating intermolecular vibrational and

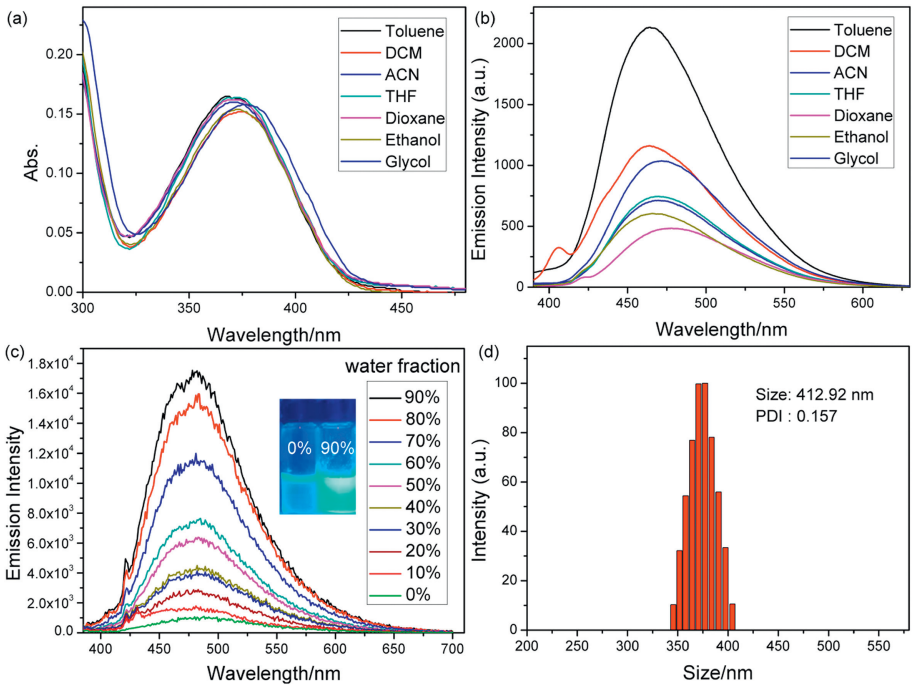

Fig. 2. (a) Absorption and (b)emission spectra of **3a** (λ_{ex}, 375 nm) in various solvents such as toluene, DCM, acetonitrile (ACN), tetrahydrofuran (THF), ethanol and ethylene glycol (glycol), respectively. (c) Emission spectra of compound **3a** in THF/water mixtures (50 μmol/L) with varied volumetric fractions of water (f_w). (d) Grain size of compound **3a** in $f_w = 90\%$.

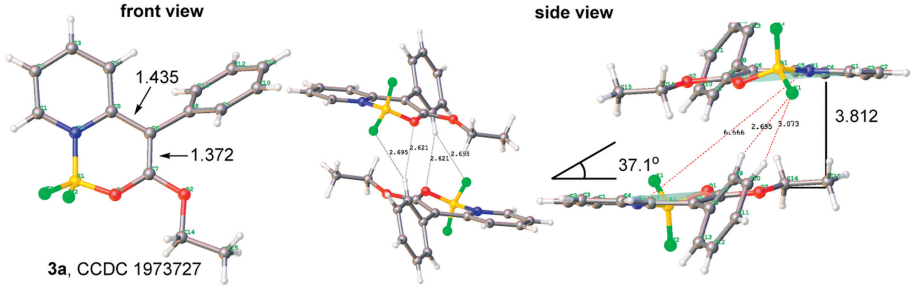

Fig. 3. Crystal-packing pattern of **3a** between the adjacent interlayered crystals from front and side view. H, light gray; C, gray; N, blue; O, red; F, green; B, yellow.

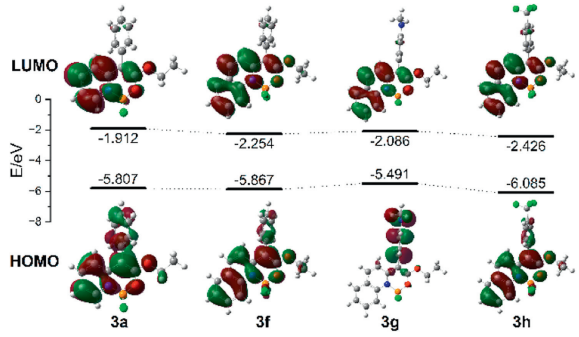

Fig. 4. Relative energies of the frontier orbitals, and DFT-predicted frontier orbitals for compounds **3a**, **3f-3h**.

rotational modes to mitigate nonradiative energy dissipation pathways, thereby enabling the enhanced radiative in the solid-state fluorescence [56].

Density functional theory (DFT) calculations on **3a**, **3f-3h** were performed using the Gaussian 09 software package. All geometrical structures were optimized and molecular orbitals calculated at the B3LYP/6–31G* level. The HOMO and LUMO plots are given in Fig. 4 and Fig. S14 (Supporting information). The LUMO of each molecule is mainly localized on the pyridine and the six-membered boron-containing heterocycles. The HOMOs of **3a**, **3f** and **3g** delocalize over the whole molecules, whereas the electron cloud distribution of the HOMO in **3g** mainly localize on the dimethylaniline moiety. Compared to **3a**, the LUMO of **3f** is lowered due to the expanded π-conjugation of the quinoline *versus* pyridine. Substitution with the dimethylaniline group is predicted to increase the HOMO and LUMO energy levels of **3g** by 0.376 eV and 0.168 eV, respectively, thereby decreasing the net HOMO-LUMO gap and redshifts the absorption when compared to **3f** (Table S4 in Supporting information) [62]. Overall, the computational results are consistent with the experimental spectroscopic observations.

The post-complexation modification was explored to further demonstrate the application value [63,64]. **3f-Cl** readily underwent both the Pd-catalyzed C–C and C–N coupling reaction to give complex **4** and **5** in 68% and 53% yield, respectively (Scheme 3a, Fig. S2 in Supporting information). In addition to conjugated skeleton, boron atom and ester group could also be divergently functionalized. We first conducted the nucleophilic substitution reaction between 4-methylphenylmagnesium bromide and **3f**, obtaining the tetra-substituted boron complex **6**. Due to the steric hindrance and electron-donating effect of the phenyl group [65], it exhibited strong emission in the solid-state and displayed red-shifted emission spectra when compared to **3f**. Interestingly, when

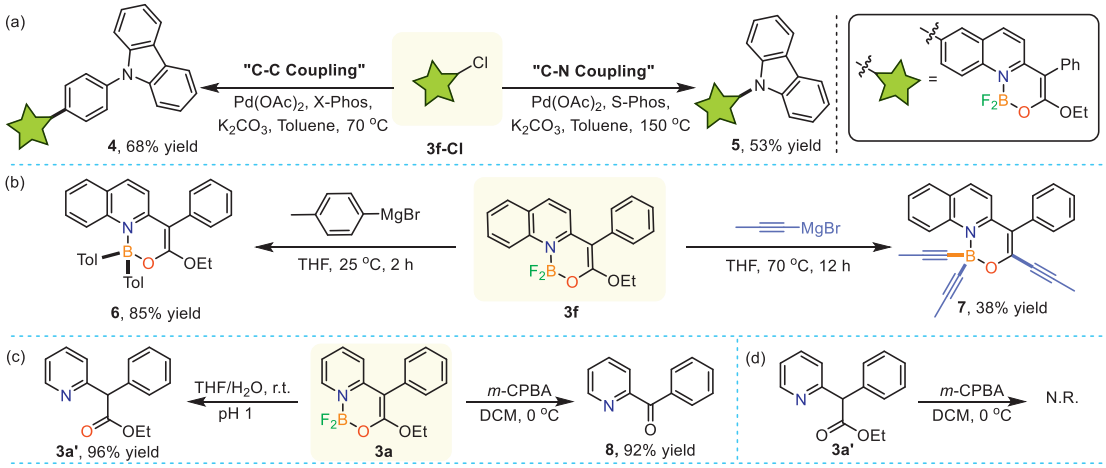

Scheme 3. Synthetic applications.

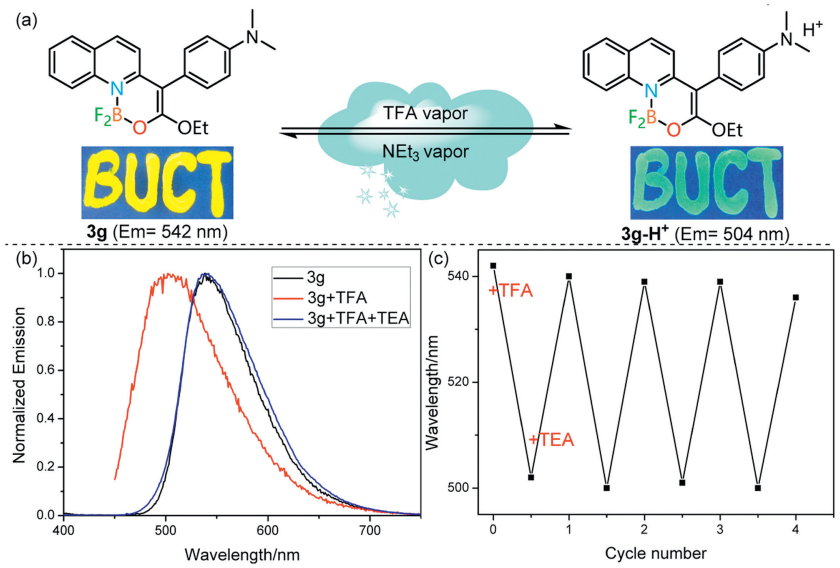

Fig. 5. (a) Reversible fluorescence switch of **3g** under conditions of TFA and TEA fumigation. (Insert picture: "BUCT" scribbled on filter paper with **3g** under 365 nm). (b, c) Spectra of **3g** before and after fumigation by TFA and TEA.

3f was reacted with excess amount of propynylmagnesium bromides [66] the ethoxy group, in addition to the fluorine atom, was also propargylated to give the unexpected triple-modified complex **7** (Scheme 3b, Fig. S3 in Supporting information). The exemplificative downstream modifications further indicated the synthetic versatility of our boron fluorophore, empowering fast acceleration for the SAR studies and resulting application-oriented research.

Stability testing was conducted on compound **3a**, revealing that it possesses good photostability and thermostability (Fig. S4 in Supporting information). Furthermore, **3a** exhibited a broad range of chemo-stability with pH ranging from 3 to 11. Nonetheless, in congruence with typical BODIPYs, **3a** decomposed to **3a′** at pH 1 conditions, resulting no fluorescence. Simultaneously, the absorption and emission spectra of solution exhibited a blue shift, indicating a decrease in molecular conjugation in **3a′** (Scheme 3c, Fig. S5 in Supporting information). Interestingly, the C=C bond in the molecule coordinated with BF_2 can undergo oxidative cleavage upon treatment with *m*-CPBA, leading to the formation of ketone **8**, whereas **3a′** remains unchanged under the same conditions (Schemes 3c and d). Again, the coordination of boron promotes the ester enolization, leading to the formation of a more reactive double bond that can be oxidized [67], and this unique pathway could potentially serve as a model for cleavage-based detection assays.

In view of its exceptional stability, we then conducted an exemplificative fluorescence-monitoring experiment employing **3g**, in the presence of acids and bases (Fig. 5, Fig. S6 in Supporting information). When subjected to UV irradiation, **3g** exhibited a yellow fluorescence. After exposing to trifluoroacetic acid (TFA) vapor, the fluorescence emission undergoes a fast shift to cyan. The mass spectrometry result ($m/z = 383.1739$) indicated that **3g** was protonated in acidic vapors (Fig. S13 in Supporting information). Despite a slight decrease in emission intensity, the cyclic protonation and deprotonation process enabled by alternating acid and base treatments allows for reversible modulation of fluorescence colors.

In summary, we have successfully designed and synthesized a series of *N*-heteroarene-ester enolate based organoboron complexes endowed with AIE characteristics. These novel scaffolds exhibited robust fluorescence, substantial Stokes shift, and outstanding photo/pH stability. X-ray crystallographic analysis revealed that the weak intermolecular interactions, namely C–H···F and C–H···O, stabilized the molecular conformations of these BF_2 chelates, thereby accounting for their pronounced fluorescence in the solid state. DFT calculations demonstrated that the both

substituents and π-conjugation have a significant impact on the emission properties. The unique structural attributes of these complexes further allowed for versatile downstream derivatization reactions, thereby opening avenues for rapid exploration of the structural diversity. Furthermore, the emission of the complex showed reversible changes when exposed to acidic gas, paving the way for future research on fluorescent sensors.

Declaration of competing interest

The authors declare that they have no known competing financial interests or personal relationships that could have appeared to influence the work reported in this paper.

Acknowledgment

J. Tan (BUCT) is grateful for the support by the National Natural Science Foundation of China (Nos. 21702013, 22271010).

Supplementary materials

Supplementary material associated with this article can be found, in the online version, at doi:10.1016/j.cclet.2024.109532.

References

[1] X.L. Yang, G.J. Zhou, W.Y. Wong, et al., Chem. Soc. Rev. 44 (2015) 8484–8575.
[2] R. Furue, T. Nishimoto, I.S. Park, et al., Angew. Chem. Int. Ed. 55 (2016) 7171–7175.
[3] H. Uoyama, K. Goushi, K. Shizu, et al., Nature 492 (2012) 234–238.
[4] Z. Yang, T. Xu, H. Li, et al., Chem. Rev. 123 (2023) 11047–11136.
[5] W. Sheng, F. Lv, B. Tang, et al., Chin. Chem. Lett. 30 (2019) 1825–1833.
[6] T. Kowada, H. Maeda, K. Kikuchi, Chem. Soc. Rev. 44 (2015) 4953–4972.
[7] J. Zhao, K. Xu, W. Yang, et al., Chem. Soc. Rev. 44 (2015) 8904–8939.
[8] J. Wang, Q. Gong, L. Jiao, et al., Coord. Chem. Rev. 496 (2023) 215367.
[9] Z. Wang, X. Teng, C. Lu, Anal. Chem. 87 (2015) 3412.
[10] Q. Gong, X. Zhang, W. Li, et al., J. Am. Chem. Soc. 144 (2022) 21992–21999.
[11] F. Ito, T. Nagai, Y. Ono, et al., Chem. Phys. Lett. 435 (2007) 283–288.
[12] D. Frath, J. Massue, G. Ulrich, et al., Angew. Chem. Int. Ed. 53 (2014) 2290–2310.
[13] Z. Chi, X. Zhang, B. Xu, et al., Chem. Soc. Rev. 41 (2012) 3878–3896.
[14] J. Mei, Y. Hong, J.W.Y. Lam, et al., Adv. Mater. 26 (2014) 5429–5479.
[15] Z. He, C. Ke, B.Z. Tang, ACS Omega 3 (2018) 3267–3277.
[16] C. Chen, C.Z. Du, X.Y. Wang, Adv. Sci. 9 (2022) 2200707.
[17] G. Meng, J. Zhou, T. Huang, et al., Angew. Chem. Int. Ed. 62 (2023) e202309923.
[18] J. Luo, Z. Xie, J.W.Y. Lam, et al., Chem. Commun. 55 (2001) 1740–1741.
[19] N.L.C. Leung, N. Xie, W. Yuan, et al., Chem. Eur. J. 20 (2014) 15349–15353.
[20] Z. He, E. Zhao, J.W.Y. Lam, B.Z. Tang, Aggregation-Induced Emission: Materials and Applications, 1, American Chemical Society, 2016, pp. 5–20.
[21] F. Zhang, X. Wu, B. Liu, et al., Coord. Chem. Rev. 493 (2023) 215337.
[22] W. Che, L. Zhang, Y. Li, et al., Anal. Chem. 91 (2019) 3467–3474.
[23] J. Zhuang, Y. Yu, R. Su, et al., Dyes Pigments 208 (2023) 110809.
[24] G. Yang, Y. Ran, Y. Wu, et al., Aggregate 3 (2022) e127.
[25] T. Zhou, R. Hu, L. Wang, et al., Angew. Chem. Int. Ed. 59 (2020) 9952–9956.
[26] E. Bodio, C. Goze, Dyes Pigments 160 (2019) 700–710.
[27] J. Mei, N.L.C. Leung, R.T.K. Kwok, et al., Chem. Rev. 115 (2015) 11718–11940.
[28] H. Wu, X. Guo, C. Yu, et al., Dyes Pigments 176 (2020) 108209.
[29] L.J. Patalag, M. Loch, P.G. Jones, et al., J. Org. Chem. 84 (2019) 7804–7814.
[30] Y. Guo, L. Zhang, C. Li, et al., J. Org. Chem. 86 (2021) 12507–12516.
[31] M. Liu, S. Ma, M. She, et al., Chin. Chem. Lett. 30 (2019) 1815–1824.
[32] Z. Yu, Y. Wu, L. Xiao, et al., J. Am. Chem. Soc. 139 (2017) 6376–6381.
[33] C. Yu, X. Fang, Q. Wu, et al., Org. Lett. 22 (2020) 4588–4592.
[34] D. Yang, P. Liu, T. Bai, et al., Macromolecules 53 (2020) 3339–3348.
[35] A.M. Grabarz, B. Jędrzejewska, A. Zakrzewska, et al., J. Org. Chem. 82 (2017) 1529–1537.
[36] B. Jędrzejewska, A. Skotnicka, A.D. Laurent, et al., J. Org. Chem. 83 (2018) 7779–7788.
[37] G. Tan, I. Maisuls, F. Strieth-Kalthoff, et al., Adv. Sci. 8 (2021) 2101814.
[38] M.A. Potopnyk, R. Lytvyn, Y. Danyliv, et al., J. Org. Chem. 83 (2018) 1095–1105.
[39] Y. Chen, Z. Liao, T. Cao, et al., Green Synth. Catal. 3 (2022) 89–94.
[40] A.C. Murali, P. Nayak, S. Nayak, et al., Angew. Chem. Int. Ed. 62 (2023) e202216871.
[41] Z. Zhang, H. Bi, Y. Zhang, et al., Inorg. Chem. 48 (2009) 7230–7236.
[42] C. Yu, E. Hao, X. Fang, et al., J. Mater. Chem. C 7 (2019) 3269–3277.
[43] D. Frath, S. Azizi, G. Ulrich, et al., Org. Lett. 13 (2011) 3414–3417.
[44] N. Zhao, C. Ma, W. Yang, et al., Chem. Commun. 5 (2019) 8494–8497.
[45] G. Tan, M.L. Schrader, C. Daniliuc, et al., Angew. Chem. Int. Ed. 59 (2020) 21541–21545.
[46] C. Yu, X. Fang, H. Wang, et al., J. Org. Chem. 86 (2021) 11492–11501.
[47] R. Yoshii, A. Nagai, K. Tanaka, et al., Chem. Eur. J. 19 (2013) 4506–4512.
[48] R. Yoshii, A. Hirose, K. Tanaka, et al., J. Am. Chem. Soc. 136 (2014) 18131–18139.
[49] P. Su, L. Wen, Y. Zhou, et al., Chem. Eur. J. 28 (2022) e202201372.
[50] Y. Kubota, H. Hara, S. Tanaka, et al., Org. Lett. 13 (2011) 6544–6547.
[51] C. Wu, W. Liu, K. Li, et al., Angew. Chem. Int. Ed. 60 (2021) 3994–3998.
[52] S. Luo, J. Wang, N. Li, et al., Angew. Chem. Int. Ed. 62 (2023) e202310943.
[53] X.F. Song, C. Jiang, N. Li, et al., Chem. Sci. 14 (2023) 12246–12254.
[54] C. Jin, K. Xu, X. Fan, et al., Chin. Chem. Lett. 31 (2020) 91–94.
[55] J. Huang, L. Bourda, S. Tusupbayev, et al., Dyes Pigments 217 (2023) 111374.
[56] X. Wang, F. Qi, Z. Jiang, et al., Dyes Pigments 186 (2021) 108999.
[57] H. Yang, K. Ye, J. Sun, et al., Asian J. Org. Chem. 6 (2017) 199–206.
[58] Z. Huang, A. Ding, J. Yang, et al., Chem. Eur. J. 29 (2023) e202203628.
[59] C. Yu, L. Jiao, H. Yin, et al., Eur. J. Org. Chem. 28 (2011) 5460.
[60] S. Zhang, Y. Huang, L. Kong, et al., Dyes Pigments 181 (2020) 108574.
[61] P. Sykes, A Guidebook to Mechanism in Organic Chemistry, 5th edn, 1981.
[62] Y. Zhang, A. Ding, S. Guo, et al., J. Mater. Chem. C 10 (2022) 6078–6084.
[63] J. Chen, S. liu, S. Su, et al., Sci. Adv. 9 (2023) eadi1370.
[64] X. Peng, K. Xu, Q. Zhang, et al., Trends Chem. 4 (2022) 643–657.
[65] A.B. More, S. Mula, S. Thakare, et al., J. Org. Chem. 79 (2014) 10981–10987.
[66] L. Li, Y. Gao, C. Dou, et al., Chin. Chem. Lett. 31 (2020) 1193–1196.
[67] F.V. Singh, H.M.S. Milagre, M.N. Eberlin, et al., Tetrahedron Lett. 50 (2009) 2312–2316.